Scaling of plasma temperature, density, size, and x-ray emission above 1 keV with array diameter and mass for aluminum imploding-wire plasmas

M. Gersten, W. Clark, J. E. Rauch, G. M. Wilkinson, J. Katzenstein,* and R. D. Richardson†
Maxwell Laboratories, Inc., San Diego, California 92123

J. Davis, D. Duston, J. P. Apruzese, and R. Clark
Naval Research Laboratory, Washington, D.C. 20390
(Received 26 July 1984; revised manuscript received 8 July 1985)

A series of five aluminum imploding-wire experiments were performed to investigate the dependence of plasma temperature, density, size, and x-ray emission above 1 keV on the initial wire-array diameter and mass per unit length. The plasmas were created by imploding cylindrical arrays of fine wires with the Blackjack 5 pulse generator. In these experiments the array diameter and mass per unit length were varied by factors of 2 and 4.5, respectively. The electron temperatures were determined from the slope of the free-to-bound continuum, the intensity ratios of selected x-ray-emission lines and strength of the continuum edges. The line ratios were interpreted by means of a collisional radiative equilibrium model. Plasma ion densities were obtained from the total x-ray emission above 1 keV. The size of the plasma that emits above 1 keV was inferred from x-ray pinhole photographs and from measurements of the line broadening caused by the finite source size. As the initial diameter of the wire array was increased, the array mass was decreased in order to maintain constant implosion time and optimum energy coupling from the pulse generator to the load. The larger-diameter, lower-mass arrays produced larger-diameter, higher-temperature, lower-density plasma pinches. With the simultaneous increase in array diameter and decrease in array mass, the electron temperature increased from 0.5 to 0.8 keV, the ion density decreased from 4×10^{19} to 0.13×10^{19} cm^{-3}, the diameter of the plasma column increased from 1.2 to 5.5 mm, and the x-ray emission above 1 keV decreased from 20 to 0.45 kJ.

I. INTRODUCTION

The spectroscopy of single exploding-wire plasmas,[1-3] multiple imploding-wire-array plasmas,[1,4-6] and gas-jet plasmas[7] has been investigated in some detail. The electron temperature, ion density, and size of the pinch created by imploding plasmas have been characterized for several different elements for a limited range of initial array parameters. The variation of electron temperature with driving power for constant array conditions has been described for titanium plasmas,[8] as has the temperature scaling in aluminum plasmas, when the initial array diameter is held constant and the mass per unit length is varied.[9] However, changing the mass per unit length while holding the array diameter constant can result in significant changes in the coupling between the pulse generator and the imploding-wire load.[10] In this formulation, the coupling of power and energy from a pulse generator to an imploding-plasma load may be calculated in terms of the dimensionless variables

$$A=\frac{1}{2}\left[\frac{N-1}{N}\right]^3\left[\frac{\mu_0}{2\pi}\right]^3\frac{V_0^2}{Z_0^4}\left[\frac{l}{r_0}\right]^2\frac{1}{m}\ ,\quad B=\frac{2\pi L_p}{\mu_0 l}\ .$$

In these expressions, the quantity V_0 is the rms open-circuit voltage, Z_0 is the characteristic impendence, N is the number of wires, l, r_0, and m are the length, initial radius, and total mass per unit length of the wire array, and L_p is the sum of the inductance of the vacuum transmission line (VTL) which connects the pulser to the load and the initial (resting) inductance of the load. For a given value of the parameter B, a quantity called the power-amplification factor (P_{AF}) [$P_{AF}=lm\dot{v}_f v_f/(V_0^2/4Z_0)$, where v_f is the final radial velocity of the imploding plasma], which is the ratio of the time derivative of the kinetic energy at the end of the implosion to the instantaneous power the generator could deliver to a matched load, depends only on the coupling parameter A. The P_{AF} provides a convenient measure of the coupling between an imploding plasma and the driving electrical pulse generator. For constant B, this coupling is optimized by choosing a value of the parameter A which maximizes the P_{AF}. For a constant driving power and constant imploding-plasma length, an optimum value of A can be maintained as the initial array radius is changed by keeping the product $r_0^2 m$ constant. In this paper, a series of five aluminum wire-array implosions are described, where this product was held approximately constant while the array diameter was increased by a factor of 2 and the mass unit length was decreased by a factor of 4.5. This resulted in a significant decrease in the mass involved in the implosions and a resulting increase in the amount of energy available per atom. The x-ray emission from the plasmas was analyzed to determine the effect of the changes in the array diameter and mass on the temperature, density, size of the plasma pinch, and total x-ray emission above 1 keV.

II. EXPERIMENT

The Blackjack 5 pulse generator consists of a water dielectric pulse line driven by a 2.1-MJ oil-insulated Marx generator.[11] At full power the generator produces ~10 TW of electrical power. For a typical imploding-plasma load with ~20 nH inductance in the VTL, the generator produces a peak voltage at the entrance to the VTL of ~3.0 MV. This peak is followed ~40 ns later by a peak current of ~4.6 MA. For the experiments described here, the generator was operated at a nominal peak power of ~4.5 TW. The generator load consisted of a cylindrical array of aluminum wires located at the center of the converging VTL geometry. The current from the pulse generator ionized the aluminum wires and caused them to implode to form a dense pinch near the axis of the cylindrical array fixture. As described above, the array diameter and mass were chosen so that optimum energy coupling was obtained between the pulse generator and the plasma load.

Spectra of the x-ray emission above 1 keV from the imploding plasmas were measured with a KAP (KAP denotes potassium acid phthalate) convex curved crystal spectrograph. The radiation was simultaneously diffracted by the (001), (002), and (013) planes of the KAP crystal and recorded on Kodac No-Screen x-ray film. The exposures were converted into relative intensities by taking into account the film response,[12,13] filter transmission,[14] crystal efficiency,[15] and experimental geometry.

The total x-ray emission above 1 keV, which corresponds mostly to K-shell transitions, was measured with a thin-foil calorimeter (0.42 g/cm^2 tantalum) using a fine-wire (0.025 mm in diameter) Chromel-Constantan thermocouple temperature sensor. In order to discriminate between the large amounts of radiation produced at photons energies below that of the K-shell regime, a composite filter of 0.567 mg/cm^2 polycarbonate (aluminized) and 0.879 mg/cm^2 Mylar (aluminized) was used between the source and calorimeter. The effective transmission of a typical aluminum spectrum above 1 keV, such as that shown in Fig. 4, through this filter was about 0.5. The fluence measured in this manner was viewed at right angles to the axis of the plasma pinch and the equivalent source strength was obtained by multiplying the filter-transmission corrected fluence by 4π times the distance squared.

The electron temperatures in the plasma were determined from the slope of the free-to-bound continuum and from comparison of the values of measured and calculated line ratios. The temperature-sensitive line ratios used were the ratio of the H-like ($1s-2p\ ^2P$) to He-like ($1s^2-1s\,2p\ ^1P$) and the H-like ($1s-3p\ ^2P$) to He-like ($1s^2-1s\,5p\ ^1P$) transitions.

For aluminum emission above 1 keV and the convex geometry used in the spectrograph, the (001) plane of the potassium acid phthalate (KAP) crystal has low resolution and low reflectivity. However, the radiation diffracted by the (001) plane is not overlapped by radiation diffracted by other planes. This latter feature is important for measurements of electron temperature from the slope of the free-to-bound continuum. The (002) plane is characterized by medium resolution and low reflectivity, and the (013) plane by high resolution and high reflectivity. By making use of all three planes, an optimum combination of resolution, lack of overlapping orders, and redundancy for cross-checking measurements can be achieved. Based on this approach, the slope of the free-to-bound continuum was determined from the (001) plane, the $\mathcal{I}_{\text{H-like}}(1s-2p\ ^2P)/\mathcal{I}_{\text{He-like}}(1s^2-1s\,2p\ ^1P)$ intensity ratios were determined separately from the (002) and (013) planes, and the $\mathcal{I}_{\text{H-like}}(1s-3p\ ^2P)/\mathcal{I}_{\text{He-like}}(1s^2-1s\,5p\ ^1P)$ intensity ratios were determined separately from the (013) and (001) planes. The line ratios given in Table III are averages of measurements from two planes, and the corresponding error bars are the deviations of the two separate measurements from the average. Where no error bar is given, the line ratio was available from only one plane. The error bars in the temperature measurement correspond to the error bars associated with the line ratios.

The theoretical calculations of line ratios assume an isothermal, isodense plasma in collisional-radiative equilibrium (CRE) and take into account opacity effects.[16] Calculations of line ratios as a function of temperature were performed for each of the five cases studied experimentally. The size of the plasma column as determined from x-ray pinhole photography and the ion density, as determined from the total x-ray emission above 1 keV, were used in computing opacity effects. The calculated line ratios are shown in Figs. 1 and 2. The differences between the five curves (four curves in Fig. 2) are due primarily to varying collisional and opacity effects for each of the implosions. For the plasma discussed here, the optical depth at the center of the Al XII $1s^2-1s\,2p\ ^1P$ line is between 32 and 155 (see Table IV).

To compute the synthetic spectra we have used a multifrequency radiative transfer model.[17] It differs from the line-ratio calculations in that the spectral lines and the continuum are subdivided into many frequencies to allow self-consistent computation of continuum slopes and line-continuum interactions. Frequency-integrated escape

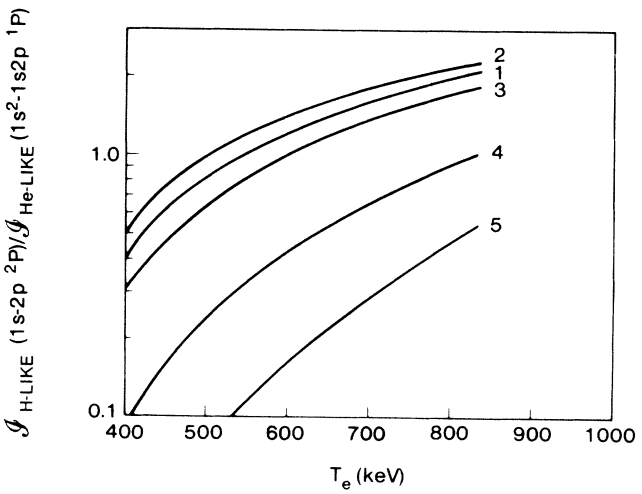

FIG. 1. $\mathcal{I}_{\text{H-like}}(1s-2p\ ^2P)/\mathcal{I}_{\text{He-like}}(1s^2-1s\,2p\ ^1P)$ line ratio versus electron temperature for the implosions discussed. The calculations take opacity effects into account and were performed for each case individually using the density and size information given in Tables III and IV.

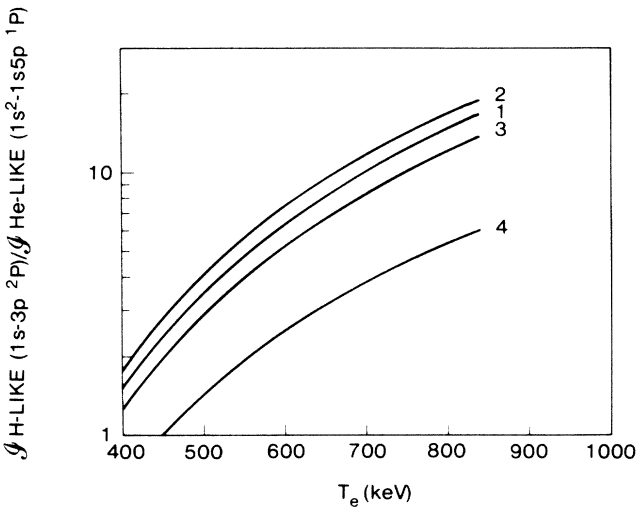

FIG. 2. $\mathcal{J}_{\text{H-like}}(1s-3p\ ^2P)/\mathcal{J}_{\text{He-like}}(1s^2-1s\,5p\ ^1P)$ line ratio versus electron temperature for the implosions discussed. The calculations take opacity effects into account and were performed for each case individually using the density and size information given in Tables III and IV.

probabilities are not employed in these latter studies (since they are not necessary with a multigroup approach), but angular effects in cylindrical geometry are treated for each frequency using the algorithm of Ref. 18.

The ion densities were determined by comparing the total x-ray emission above 1 keV measured by thermocouple calorimeters with the total x-ray emission above 1 keV as a function of ion density calculated from the collisional-radiative model. These calculations used measured values of electron temperature, size of emitting plasma, and x-ray pulse duration. Another technique which has been used in the past to determine density involves measurements of density-sensitive line ratios. Examples of this technique include measurement of the intensity ratio of the dielectronic satellites[19–21] $\mathcal{J}_{\text{He-like}}(1s\,2p\ ^3P-2p^2\ ^3P)/\mathcal{J}_{\text{He-like}}(1s\,2p\ ^3S-2s\,2p\ ^3P)$ and measurement of the He-like resonance to intercombination[19,22] $\mathcal{J}_{\text{He-like}}(1s^2-1s\,2p\ ^1P)/\mathcal{J}_{\text{He-like}}(1s^2-1s\,2p\ ^3P)$ intensity ratio. However, the dielectronic satellites cannot be used for aluminum for ion densities below $\sim 10^{20}$ cm^{-3}. The latter line ratio can be useful for aluminum for ion densities above 10^{19} cm^{-3}. However, intense satellite lines, which are unresolved from the resonance line and the multivalued density determination in optically thick plasmas,[22] introduce large uncertainties. Since some implosions involved ion densities less than 10^{19} cm^{-3}, and opacity effects were large, the line-ratio methods were not useful in these experiments. The series-merging technique[23–25] has been used to estimate densities based on Stark broadening.[2,4,7] However, because the size of the plasma was large in some of the experiments reported here, the line broadening due to the finite size of the plasma source was larger than that due to Stark broadening.[26] As a result, the series-merging technique could not be used.

The size of the plasma column that corresponds to x-ray emission above 1 keV was estimated from x-ray pinhole photographs. The lateral extent of the plasma was estimated from the line broadening caused by the finite source size.[26] This latter estimate was made by measuring full width at half maximum (FWHM) for two isolated spectral lines resulting from the H-like $(1s-3p\ ^2P)$ and H-like $(1s-4p\ ^2P)$ transitions. The two additional major line-broadening mechanisms for these lines are (1) line broadening due to the crystal rocking curve, and (2) Doppler broadening. By appropriately deconvolving the line broadening due to the crystal rocking curve[27] and to the Doppler effect, and by using the formula in Ref. 26, the lateral extent of the plasma was obtained. It is slightly larger than the plasma diameter as determined from x-ray pinhole photographs. This is to be expected since kinks in the plasma column increase the effective width as determined from source-size broadening.

III. RESULTS

Table I summarizes the normalized initial wire-array diameter d_0 and normalized mass per unit length m for the five aluminum imploding-wire shots of interest. Also

TABLE I. Normalized initial wire-array diameter, d_0, and normalized mass per unit length, m, for five aluminum imploding-wire experiments. Also shown are measured peak values of the voltage at the entrance to the VTL, $V_{\max}$, and the load current, $I_{\max}$. Calculated values of the power-amplification factor, P_{AF}, are shown for optimum coupling conditions, $P_{\text{AF(max)}}$, and actual experimental conditions, $P_{\text{AF(act)}}$.

Implosion no.	d_0 (normalized)[a]	m (normalized)[b]	$V_{\max}$ (MV)	$I_{\max}$ (MA)	$P_{\text{AF(max)}}$	$P_{\text{AF(act)}}$
1	0.5	1.0	2.4	4.0	8.9	8.9
2	0.5	0.85	2.3	3.8	8.25	7.7
3	0.65	0.6	2.1	3.8	8.5	8.5
4	0.85	0.4	2.3	3.9	9.3	9.3
5	1.0	0.22	2.2	4.9	8.6	8.0
Average			2.25	3.875[c]	8.7	8.45
Standard deviation (σ)			0.1	0.08[c]	0.33	0.58

[a]Normalized is d_0 divided by d_0 of implosion no. 5.
[b]Normalized is m divided by m of implosion no. 1.
[c]Takes into account first four implosions only.

TABLE II. Final wire velocity, v_f, the calculated kinetic energy of the array, E_k, and the kinetic energy per array atom, E_{kA}, calculated at 10% of the initial array diameter for five aluminum imploding-wire experiments.

Implosion no.	v_f (10^6 m/s)	E_k (kJ)	E_{kA} (10^{-14} J)
1	0.625	80	0.9
2	0.6	64	0.8
3	0.85	90	1.6
4	1.1	94	2.7
5	1.325	80	4.0

shown are the measured peak values of the voltage at the entrance to the VTL and the load current for these shots. In addition, Table I gives the results of calculations of the peak value of the P_{AF} ($P_{AF(max)}$), which occurs when the coupling parameter is optimum ($A = A_{opt}$) and the calculated value of the P_{AF} for the experimental conditions associated with each of the implosions. The average deviation of the calculated value of the P_{AF} for these experiments from $P_{AF(max)}$ was only $\sim 3\%$. This occurred primarily because of shot to shot variations in the generator open-circuit voltage V_0. Except for the last implosion, the shot-to-shot variation in the VTL voltage and load current in the experiments was small. The last shot had a load current of 4.9 MA, which was $\sim 25\%$ higher than average. Pinhole photographs indicate that the final plasma diameter for this shot was substantially larger than for the other shots. Since the "motional impendance" due to the changing inductance of the imploding load $\dot{L}$ is proportional to $1/r$, a larger final implosion diameter would be expected to result in a lower value of $\dot{L}$ and, consequently, a higher peak current.

Table II gives calculated values of the final wire-array velocity v_f, the kinetic energy of the array, E_k, and the available kinetic energy per atom, E_{kA}, for the five shots. The calculations were performed at a radius $r = 0.1 r_0$. The calculated total kinetic energy of the array varied only by $+25\%$. However, as the diameter of the arrays was increased and the mass was decreased, the calculated final velocity and kinetic energy per atom increased by factors of 2.2 and 4.9, respectively.

The ion densities (N_i) of the plasmas as calculated from the CRE model using the measured total x-ray emission above 1 keV, the corresponding plasma size, duration of x-ray pulse, and plasma temperature, are shown in Table III. The ion density decreased from 4×10^{19} cm^{-3} for the 15-mm-diam case (implosion no. 2) to 0.13×10^{19} cm^{-3} for the 30-mm-diam case (implosion no. 5). Another quantity, the number of atoms in the array divided by the volume of the plasma, N_a (as estimated from x-ray pinhole photographs), is also given. N_a is a factor of 8 higher than N_i for implosion no. 1, and only a factor of 2 higher than N_i for implosions no. 4 and no. 5. This indicates that for the lighter arrays a larger fraction of the available ions participate in the x-ray emission above 1 keV. This is consistent with the average energy available per atom.

X-ray pinhole photographs from three imploding-plasma shots are shown in Fig. 3. The photographs show the spatial character of the x-ray-emitting region for three different array diameters. The smaller-diameter array resulted in a tightly pinched plasma column, while the larger-diameter arrays resulted in diffuse plasmas. The diameter of the plasma column (PC), as determined from the x-ray pinhole photographs, increased from 1.2 to 5.5 mm as the initial array diameter increased by a factor of 2. The effective diameter, as determined from source-size line broadening, varied from 1.8 to 6.2 mm under these conditions (Table IV).

The correlation between the size of the x-ray-emitting region, as measured from the pinhole photograph, and the lateral extent of the plasma, as measured from source-size line broadening, is good. This agreement is particularly good for the two large-diameter arrays where the lateral displacements due to kinks in the plasma column are small in comparison to the dimension of the plasma. Also, the line broadening due to the crystal rocking curve and Doppler broadening for these cases is small in comparison to the source-size line broadening.

The total x-ray emission above 1 keV decreased from 20 to 0.45 kJ, a factor of ~ 45, between implosions no. 2 and no. 5. Signals from x-ray diodes sensitive to the total x-ray emission indicate a similar decrease for the total x-ray emission. In the temperature range of interest (500—800 eV) the K-shell emission for Al XII decreases and the K-

TABLE III. Measured ion density, N_i, total number of atoms divided by the plasma volume, N_a, the plasma diameter as estimated from pinhole photographs, S_{PC}, the plasma diameter as estimated from source-size line broadening, S_L, the calculated optical depth at the center of the spectral line resulting from the He-like ($1s^2$—$1s2p\ ^1P$) transition, OD, and the x-ray emission above 1 keV, $\mathscr{E}_{x\ ray}$, for five aluminum imploding-wire experiments.

Implosion no.	N_i[a] (10^{19} cm^{-3})	N_a[a] (10^{19} cm^{-3})	S_{PC}[b] (mm)	S_L[b] (mm)	OD	$\mathscr{E}_{x\ ray}$ (>1 keV) (kJ)
1	3.4	28	1.2	1.8	132	14
2	4.0	24	1.2	1.8	155	20
3	2.2	11	1.5	2.2	121	10
4	0.7	1.4	3.3	3.6	44	4.5
5	0.13	0.3	5.5	6.2	32	0.45

[a]Uncertainty in N_i and N_a is approximately a factor of 2.
[b]Uncertainty in S_{PC} and S_L is 25%.

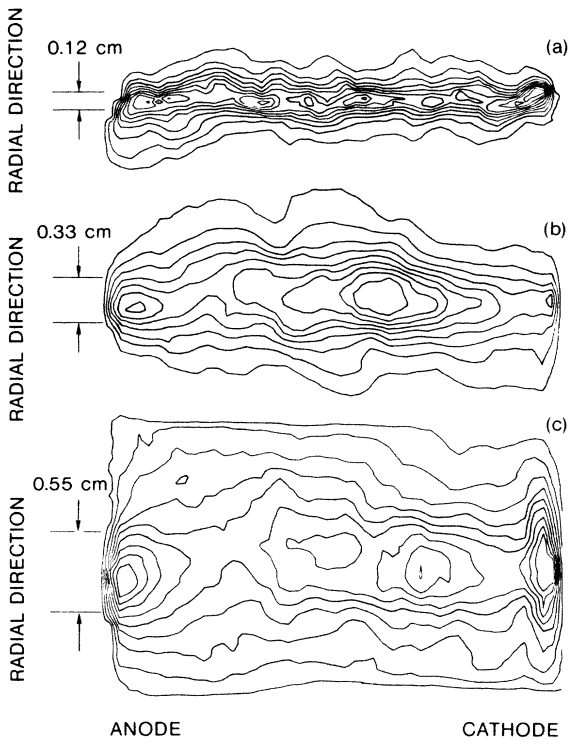

FIG. 3. Contour plots of pinhole photographs obtained from the plasma regions that radiate above 1 keV. They correspond to normalized initial array diameters of (a) 0.5, (b) 0.85, and (c) 1.

shell emission from Al XIII increases as a function of temperature. The total K-shell emission, which comprises most of the x-ray emission above 1 keV, has, therefore, a weak temperature dependence (less than a factor of 2).[16] It is, however, considerably more sensitive to the ion density N_i, and to the radial size of the plasma, as determined from pinhole photographs, S_{PC}. For densities and sizes on the order of those obtained for implosion no. 5 ($N_i = 0.13 \times 10^{19}$ cm^{-3}, $S_{PC} = 5.5$ mm), the x-ray yield above 1 keV is proportional to $N_i^2 S_{PC}^2$. For higher densities, such as those obtained for implosion no. 2 ($N_i = 4 \times 10^{19}$ cm^{-3}, $S_{PC} = 1.2$ mm), the x-ray yield above 1 keV is proportional to $N_i^{1.7} S_{PC}^{1.5}$. The reduction in the dependence of the x-ray yield on the ion density and size of the plasma column is due to opacity effects.

Table IV summarizes the electron-temperature measurements. The average electron temperature, as determined from line ratios, varied from 0.45 to 0.8 keV, and the temperature determined from the slope of the free-to-bound continuum varied from 0.55 to 0.8 keV as the array diameter was increased by a factor of 2. The temperatures obtained from the $\mathcal{I}_{\text{H-like}}(1s-2p\ ^2P)/\mathcal{I}_{\text{He-like}}(1s^2-1s2p\ ^1P)$ intensity ratios and from the $\mathcal{I}_{\text{H-like}}(1s-3p\ ^2P)/\mathcal{I}_{\text{He-like}}(1s^2-1s5p\ ^1P)$ intensity ratios are in excellent agreement. In the largest-diameter-array case, the K-shell x-ray-emission intensity was low and therefore only the temperature from the $\mathcal{I}_{\text{H-like}}(1s-2p\ ^2P)/\mathcal{I}_{\text{He-like}}(1s^2-1s2p\ ^1P)$ intensity ratio could be obtained. The temperatures obtained from the recombination continuum, however, are slightly higher than those obtained from the line-ratio measurements. This is not surprising in view of the inhomogeneous nature of the plasma and the existence of temperature gradients in the K-shell-emitting region. For example, calculations performed for a 0.5-mm-diam aluminum plasma, at an ion density of 3×10^{19} cm^{-3} (Ref. 16) show that the intensity of the bare nucleus, Al XIV, to the Al XIII recombination continuum increases by approximately an order of magnitude as the temperature increases from 500 to 800 eV. As a consequence, the Al XIV to Al XIII recombination would be expected to be characteristic of higher-temperature regions of the plasma, where Al XIV is abundant and emits efficiently, wheras the line ratios will be more indicative of cooler regions, where Al XIII and Al XII are the dominant ionization stages. Gradient effects are discussed in Ref. 16. A specific example of the differing line and continuum temperatures is discussed next.

The spectrum between 1.5 and 3.5 keV consists primarily of emission from the He-like (Al XII) and H-like (Al XIII) ionization stages in addition to satellite lines from lower ionization stages. The spectra acquired from implosions no. 2 and no. 4 with the (001) plane of the KAP crystal are shown in Figs. 4 and 5. The spectral lines resulting from the He-like ($1s^2-1s2p\ ^1P$), H-like ($1s-2p\ ^2P$), He-like ($1s^2-1s5p\ ^1P$), and H-like ($1s-3p\ ^2P$)

TABLE IV. Experimentally measured line ratios, the temperatures inferred from the measured line ratios, and the temperatures inferred from the free-to-bound continuum for five aluminum imploding-wire experiments.

Implosion no.	R_1[a]	$T_e(R_1)$ (keV)	R_2[b]	$T_e(R_2)$ (keV)	T_e (continuum) (keV)
1	0.72±0.18	0.475±0.04	2.25±0.5	0.445±0.025	0.55±0.11
2	0.85±0.03	0.470±0.01	2.31±0.14	0.430±0.008	0.55±0.12
3	0.97±0.06	0.590±0.01	4.0	0.55	0.80±0.16
4	0.91±0.05	0.795±0.02	4.94	0.785	
5	0.39	0.760			

[a] R_1 is the intensity ratio of the spectral lines resulting from the H-like ($1s-2p\ ^2P$) and He-like ($1s^2-1s2p\ ^1P$) transitions.

[b] R_2 is the intensity ratio of the spectral lines resulting from the H-like ($1s-3p\ ^2P$) and He-like ($1s^2-1s5p\ ^1P$) transitions.

transitions, which were used to determine the intensity line ratios, are marked with numbers 1–4, respectively. Because the spectral lines resulting from this He-like ($1s-2p\ ^2P$) and He-like ($1s^2-1s2p\ ^1P$) transitions are not well resolved by the (001) plane, the $\mathcal{I}_{\text{H-like}}\ (1s-2p\ ^2P)/\mathcal{I}_{\text{He-like}}(1s^2-1s2p\ ^1P)$ line ratio was obtained from the spectra acquired with the (002) and (013) planes since, as mentioned earlier, they provide much better resolution. To provide a demonstration that inhomogeneous plasmas may exhibit different line and continuum temperatures, we have computer synthetic spectra using the multifrequency radiative transfer model described in Sec. II.

Figure 4 represents the measured and calculated spectra from implosion no. 2. The inner 16% and outer 84% of the plasma volume were assigned temperatures of 650 and 300 eV, respectively. The volume and temperature partitioning were chosen based upon a number of spectral calculations using varied plasma conditions, with the objective of providing a fit to both the line and continuum radiation. The line-ratio temperatures obtained were identical to those obtained with the homogeneous escape-probability model. However, the effective continuum temperature of the calculated spectrum, 500 eV, is higher and well within the error limits of the measured continuum slope, which is 550 ± 110 eV. Therefore, the overall spectrum is consistent with that of a pinched plasma column with a relatively small high-temperature core and a much larger cooler surrounding region. This type of configuration is suggested by magnetohydrodynamics (MHD) calculations.[28] The measured ion density (4×10^{19} cm^{-3}) and the measured diameter of the hot, high-emissivity, inner plasma volume (1.2 mm) were used in the spectrum calculations. The diameter of the colder plasma was assumed to be 3 mm.

The measured spectrum of implosion no. 4 did not yield a consistent continuum temperature. However, we have calculated a spectrum based upon a similar two-temperature plasma to demonstrate that the line spectrum and continuum edges are consistent with the hot-core model. In this case the ion density and outer plasma diameter were assumed to be 0.7×10^{19} cm^{-3} and 3.3 mm, respectively, as is consistent with Table III. The temperature of the inner 16% was taken as 1500 eV, and the temperature of the outer 84% of the plasma volume was taken as 750 eV. Again, the line ratios are consistent with the previously quoted temperature of 790 eV (Table IV), even though two separate regions of considerably different temperatures are postulated. Some of the lines in the experimental spectrum do not appear in the theoretical one; this is because such lines are not included in the radiation transport model. The majority of the observed lines are modeled, however.

In addition to the line ratios of selected spectral lines and the slope of the free-to-bound continuum, the intensity of recombination edges can also serve as a temperature diagnostic. In both the calculated and the measured spectra, the Al XII recombination edge (at 2.09 keV) is markedly higher for the low-temperature implosion (no. 2) than for the high-temperature implosion (no. 4). This is due to the larger Al XII abundance.

From Tables III and IV it is clear that, although the energy-coupling efficiency from the generator to the load was kept constant for these experiments, the changes in the array dimensions introduced considerable changes in the average properties of the plasmas. The electron temperature increased from 0.5 to 0.8 keV, the ion density decreased from 4×10^{19} to 0.13×10^{19} cm^{-3}, and the diameter of the plasma column increased from 1.2 to 5.5 mm, and the x-ray yield above 1 keV increased from 20 to 0.45 kJ. Computer simulations indicate that the plasma behavior, after the wires assemble on axis, is complex and may involve several compression cycles. During these cycles, the high-density plasma would radiate, causing the temperature to decrease due to radiative cooling. The de-

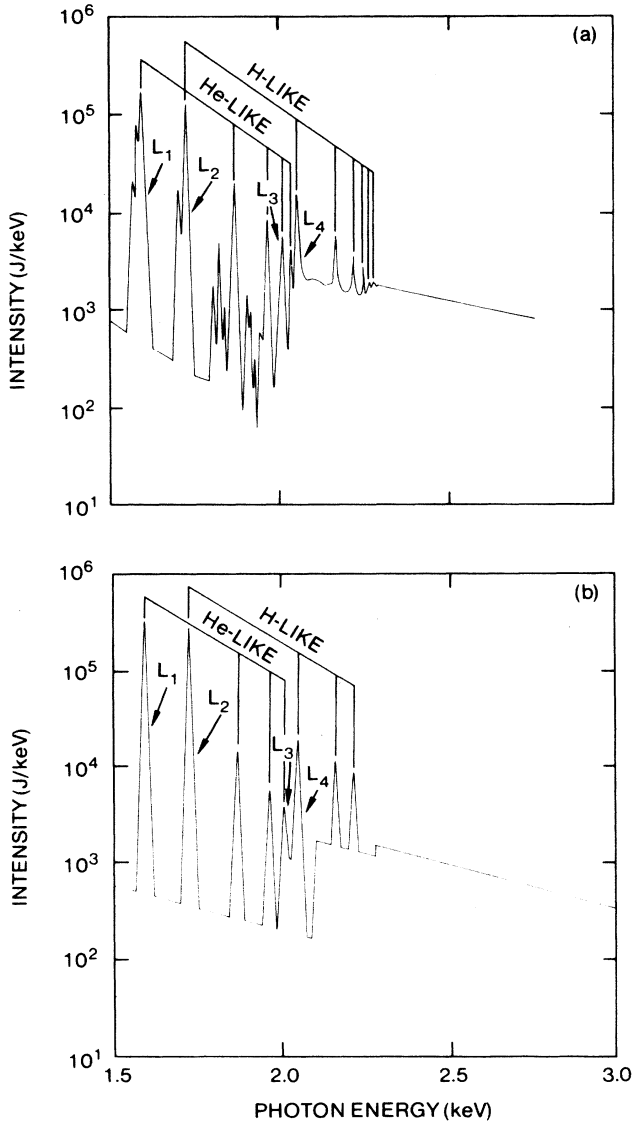

FIG. 4. Comparison of measured (top) and calculated (bottom) spectra for implosion no. 2. Plasma conditions assumed in the calculation are described in the text. Experiment broadening of 16 eV has been convolved with the spectrum. L_1, L_2, L_3, and L_4 are the spectral lines resulting from the He-like ($1s^2-1s2p\ ^1P$), H-like ($1s-2p\ ^2P$), He-like ($1s^2-1s5p\ ^1P$), and H-like ($1s-3p\ ^2P$) transitions.

crease in temperature would allow the plasma to be compressed further, resulting in an increase in density and additional radiation.[29] In the lower-mass implosions, where the kinetic energy per nuclei is expected to be large, the plasma may rebound as it begins to thermalize. The higher temperatures may reverse the implosion too soon and prevent compression to densities sufficient for appreciable radiation.[30] Differences in the degree of turbulent heating during the run-in phase are another, more likely, explanation for the differences in the properties of the five imploding-wire plasmas discussed here.[31] During the run-in phase the wires heat up, ionize, and accelerate toward the center of the array. If the drift velocity of the ions exceeds the speed of sound in the individual wire plasmas, turbulent heating will occur. The heating results in an expansion of the individual wire plasmas. The degree of expansion is related to the degree of turbulent heating. Turbulent heating is expected to occur in all five implosions. However, the degree of turbulent heating is larger for the low-mass arrays and may cause the individual wire plasmas to have larger diameters and lower densities during the run in phase. When the wire plasmas collide on axis, the result is a low-density plasma pinch. The low-density plasma is an inefficient radiator. With limited radiative cooling, a higher plasma temperature and reduced compression are to be expected. Such a behavior is consistent with the experimental observations, and is discussed in detail in Ref. 31.

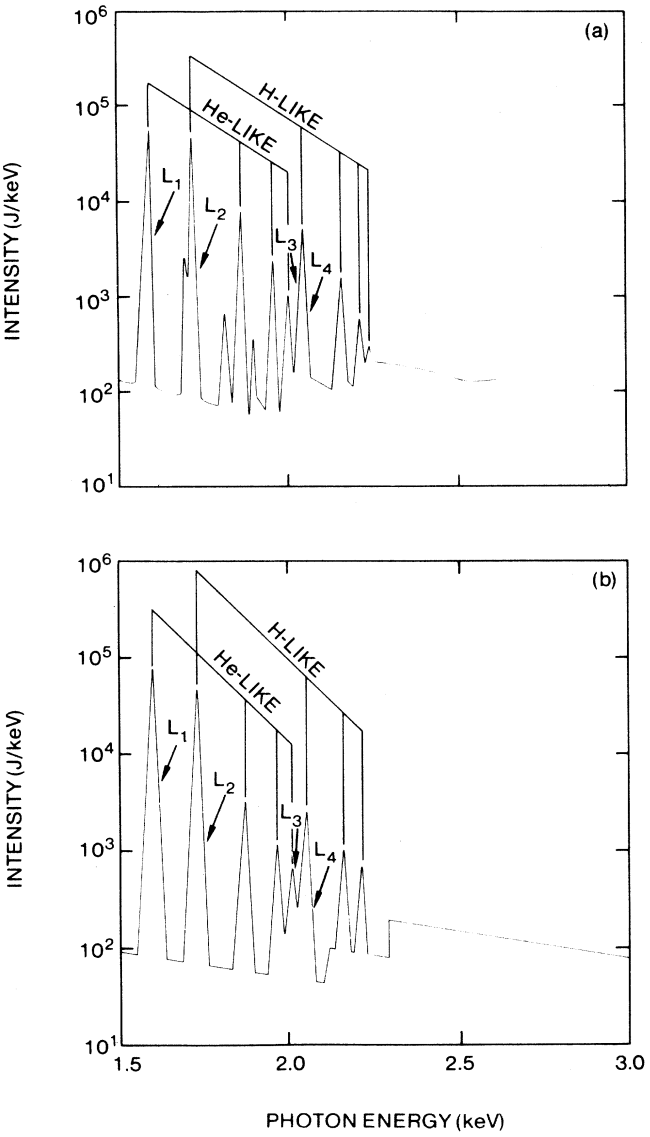

FIG. 5. Comparison of measured (top) and calculated (bottom) spectra for implosion no. 4. Plasma conditions assumed in the calculation are described in the text. Experiment broadening of 26 eV has been convolved with the spectrum. L_1, L_2, L_3, and L_4 are the spectral lines resulting from the He-like ($1s^2-1s2p\ ^1P$), H-like ($1s-2p\ ^2P$), He-like ($1s^2-1s5p\ ^1P$), and H-like ($1s-3p\ ^2P$) transitions.

IV. SUMMARY

The dependence of the electron temperature, the ion density, the diameter of the emitting plasmas, and the total x-ray emission above 1 keV on initial array parameters has been investigated for aluminum imploding-wire plasmas. As the array parameters were varied, the product of the array mass per unit length and the square of the array diameter was held constant in order to maintain optimum energy coupling between the imploding-wire load and the pulse generator, as expressed by the criterion of maximizing the power-amplification factor. As the initial diameter of the wire array was increased by a factor of 2, the temperature of the plasma pinch increased from 0.5 to 0.8 keV, the density decreased from 4×10^{19} to 0.13×10^{19} cm^{-3}, the diameter of the plasma increased from 1.2 to 5.5 mm, and the x-ray yield above 1 keV decreased from 20 to 0.45 kJ.

In the lower-mass implosions, where the kinetic energy per nuclei is expected to be large, the plasma may rebound as it collides on axis and begins to thermalize. This will result in a large, high-temperature, low-density, low-emissivity plasma, and is one possible explanation of our observations. Another possible explanation is the larger turbulent heating during the run in phase that is calculated for the lower-mass implosions. This will cause the expansion of the individual wires, which upon collision on axis will compress poorly. This also results in a large, high-temperature, low-density, low-emissivity plasma. Both of these effects can occur simultaneously.

The ability to vary the plasma parameters, as demonstrated here, can be extended to both higher and lower masses and diameters to produce even larger changes in the electron temperature and density and, in more extreme cases, to produce significant changes in the distribution of ionization stages.

ACKNOWLEDGMENT

This work was supported by the Defense Nuclear Agency under Contract No. DNA001-83-C-0007.

*Present address: University of California, Irvine, California 92717.

†Present address: Science Applications, Inc., Albuquerque, New Mexico 87109.

[1]P. G. Burkhalter, R. Schneider, C. M. Dozier, and R. D. Cowan, Phys. Rev. A **18**, 718 (1978).

[2]P. G. Burkhalter, C. M. Dozier, and D. J. Nagel, Phys. Rev. A **15**, 707 (1977).

[3]P. G. Burkhalter, C. M. Dozier, C. Stallings, and R. D. Cowan, J. Appl. Phys. **49**, 1092 (1978).

[4]P. G. Burkhalter, J. Davis, J. Rauch, W. Clark, G. Dahlbacka, and R. Schneider, J. Appl. Phys. **50**, 705 (1979).

[5]M. Gersten, J. E. Rauch, H. Reyburn, J. C. Riordan, and J. S. Pearlman, Bull. Am. Phys. Soc. **25**, 991 (1980).

[6]W. Clark, M. Gersten, J. Katzenstein, J. E. Rauch, R. D. Richardson, and G. M. Wilkinson, J. Appl. Phys. **53**, 4099 (1982).

[7]P. G. Burkhalter, J. Shiloh, A. Fisher, and R. D. Cowan, J. Appl. Phys. **50**, 4532 (1979).

[8]M. Gersten, J. E. Rauch, W. Clark, R. D. Richardson, and G. M. Wilkinson, Appl. Phys. Lett. **39**, 148 (1981).

[9]M. Gersten, J. C. Riordan, J. E. Rauch, and J. S. Pearlman, Maxwell Laboratory Report No. 1376 (1983) (unpublished).

[10]J. Katzenstein, J. Appl. Phys. **52**, 676 (1981).

[11]A. R. Miller, in *Digest of Technical Papers, 3rd IEEE International Pulse Power Conference, Albuquerque, NM, 1981* edited by T. H. Martin and A. H. Guenther (IEEE, New York, 1981).

[12]D. B. Brown, J. W. Criss, and L. S. Birks, J. Appl. Phys. **47**, 3722 (1976).

[13]C. M. Dozier, D. B. Brown, L. S. Birks, P. B. Lyons, and R. F. Benjamin, J. Appl. Phys. **47**, 3731 (1976).

[14]W. H. McMaster, N. Kerr Del Grande, J. H. Mallett, and J. G. Hubbell, Lawrence Livermore Radiation Laboratory (University of California) Report No. UCRL-50174 (unpublished).

[15]P. G. Burkhalter, D. B. Brown, and M. Gersten, J. Appl. Phys. **52**, 4379 (1981).

[16]D. Duston, J. Davis, and P. C. Kepple, Phys. Rev. A **24**, 1505 (1981).

[17]J. P. Apruzese, P. C. Kepple, K. G. Whitney, J. Davis, and D. Duston, Phys. Rev. A **24**, 1001 (1981).

[18]J. P. Apruzese, J. Quantum Spectrosc. Radiat. Transfer **25**, 419 (1981).

[19]I. Y. Skovelev, A. V. Vinogradov, and E. A. Yokov, Phys. Scr. **18**, 78 (1978).

[20]D. Duston and J. Davis, Phys. Rev. A **21**, 932 (1980).

[21]J. F. Seeley, Phys. Rev. Lett. **42**, 1606 (1979).

[22]D. Duston and J. Davis, Phys. Rev. A **21**, 1644 (1980).

[23]A. Pannekoek, Mon. Not. R. Astron. Soc. **98**, 694 (1938).

[24]D. Inglis and E. Teller, Astrophys. J. **90**, 439 (1939).

[25]J. Davis, Naval Research Laboratory Memorandum Report No. 2655, 1973 (unpublished).

[26]M. Gersten and J. E. Rauch, J. Appl. Phys. **53**, 1297 (1982).

[27]N. G. Alexandropoulos and G. G. Cohn, Appl. Spectrosc. **28**, 155 (1974).

[28]R. E. Terry and J. Guillory, JAYCOR Report No. J800-82-001 (unpublished).

[29]E. Kane and D. Duston, Bull. Am. Phys. Soc. **26**, 1068 (1981).

[30]R. E. Terry and J. Guillory, JAYCOR Report No. J207-81-004 (unpublished); R. E. Terry (private communication).

[31]N. Pereira and N. Rostoker, in *Bulletin of the 1983 IEEE International Conference on Plasma Science* (IEEE, San Diego, 1983), Vol. 57.